Atmospheric Responses to North Atlantic SST Anomalies in Idealized Experiments. Part II: North American Precipitation

QI HU

School of Natural Resources, and Department of Earth and Atmospheric Sciences, University of Nebraska–Lincoln, Lincoln, Nebraska

MICHAEL C. VERES

Department of Atmospheric and Geological Sciences, State University of New York at Oswego, Oswego, New York

(Manuscript received 3 November 2014, in final form 27 October 2015)

ABSTRACT

This is the second part of a two-part paper that addresses deterministic roles of the sea surface temperature (SST) anomalies associated with the Atlantic multidecadal oscillation (AMO) in variations of atmospheric circulation and precipitation in the Northern Hemisphere, using a sequence of idealized model runs at the spring equinox conditions. This part focuses on the effect of the SST anomalies on North American precipitation. Major results show that, in the model setting closest to the real-world situation, a warm SST anomaly in the North Atlantic Ocean causes suppressed precipitation in central, western, and northern North America but more precipitation in the southeast. A nearly reversed pattern of precipitation anomalies develops in response to the cold SST anomaly. Further examinations of these solutions reveal that the response to the cold SST anomaly is less stable than that to the warm SST anomaly. The former is ''dynamically charged'' in the sense that positive eddy kinetic energy (EKE) exists over the continent. The lack of precipitation in its southeast is because of an insufficient moisture supply. In addition, the results show that the EKE of the short- (2–6 day) and medium-range (7–10 day) weather-producing processes in North America have nearly opposite signs in response to the same cold SST anomaly. These competing effects of eddies in the dynamically charged environment (elevated sensitivity to moisture) complicate the circulation and precipitation responses to the cold SST anomaly in the North Atlantic and may explain why the model results show more varying precipitation anomalies (also confirmed by statistical test results) during the cold than the warm SST anomaly, as also shown in simulations with more realistic models. Results of this study indicate a need to include the AMO in the right context with other forcings in an effort to improve understanding of interannual-to-multidecadal variations in warm season precipitation in North America.

1. Introduction

This is the second part of a two-part paper on atmospheric responses to North Atlantic SST anomalies associated with the Atlantic multidecadal oscillation (AMO) in idealized global model experiments under the spring equinox conditions. This part focuses on precipitation and associated dynamic processes in North America.

Warm season, especially summertime, precipitation in many regions in North America has been found, statistically, to be strongly influenced by SST variations in the North Atlantic Ocean associated with the AMO (Enfield et al. 2001; Sutton and Hodson 2005, 2007; Hu and Feng 2008; Schubert et al. 2009; Mo et al. 2009; Nigam et al. 2011). In the U.S. Great Plains, for example, summertime precipitation is below the long-term average in the decades during the warm SST phase of the AMO and above the average in the cold phase of the AMO, although deviations of varying severity from this relationship occur in time. Such deviations could result from internal processes and interactions of the AMO with other forcings of local and remote origin on interannual–decadal time scales (see section 5 in Wu and Hu 2015). These interactions also mask the true effect of the AMO on North American precipitation and prompt the following question: Is the observed relationship between variations in the SST during the

Corresponding author address: Dr. Qi Hu, 707 Hardin Hall, University of Nebraska–Lincoln, Lincoln, NE 68583-0987.
E-mail: qihu@unl.edu

DOI: 10.1175/JCLI-D-14-00751.1

AMO and the precipitation in North America some statistical effect of other forcings occurring simultaneously with the AMO? In other words, does the AMO have its own distinct effect on atmospheric circulation and precipitation in North America? An answer to this question is essential, because it will help us identify the predictive value of the AMO and allow us to further explore variations of the AMO effect resulting from its interactions with other known forces.

An answer to this question can also help us clear up some confusion about the AMO effect on North American precipitation among previous studies. For instance, Hu and Feng (2008) showed coherent variations at multidecadal time scales between the AMO and summertime precipitation in the central and western United States, and their results were further tested in a modeling study of Hu et al. (2011). Wang et al. (2010) detailed limited regions with reduced precipitation during the warm phase of AMO in the Great Plains and areas west of the Mississippi River. Nigam et al. (2011) indicated a strong decrease in summertime precipitation in the contiguous United States during the warm phase of the AMO, with an exception in the area of Florida. The differences between these studies in regions of the United States where summertime precipitation decreases during the AMO warm phase raise the question of the strength of any deterministic effects of the AMO and also a need to address it.

Some prior studies have tried to verify the AMO's effect on North American warm season precipitation. Their results do not provide a conclusive answer, however. For example, Sutton and Hodson (2005, 2007), and Hu et al. (2011) evaluated the effects of the AMO using general circulation models (GCM) with a specified SST anomaly in the North Atlantic Ocean. While the results in Hu et al. (2011) reveal some physical processes connecting SST variations in the AMO and North American precipitation, those processes were derived from summertime conditions averaged from 20 or 50 model simulation years. Therefore, those processes could still be of a statistical nature or, at least, show no conclusive deterministic role of the AMO. This concern is especially warranted because in those simulations, there were years in which the simulated summertime precipitation was substantially off from the negative relationship between the AMO and the precipitation. Thus, whether the AMO is producing its own forcing on the North American circulation and precipitation remains elusive.

In this study, we address these questions using a GCM and a sequence of idealized experiments to isolate and identify the effects of the AMO. We start with an aquaplanet and then add idealized continents and orography in sequence. We allow an SST anomaly only in the North Atlantic Ocean and run the experiments under the perpetual spring equinox conditions. As discussed in Veres and Hu (2015, hereafter Part I), the designs of these model experiments allow them to isolate the effect of SST anomalies in the AMO. The model, the experiments, and methods used in this study are described in the next section (section 2). Major results are in section 3. Some of their important implications are discussed in section 4.

2. Experiment design and analysis methods

The analysis in this part of the study uses the same outputs from the model experiments detailed in Part I. To briefly summarize, we use the NCAR Community Earth System Model, version 1.0.5 (CESM1.0.5), which has the Community Atmospheric Model, version 5.1 (CAM5.1), coupled with the Community Land Model, version 4 (CLM4). The model horizontal resolution is T85, equivalent to 1.4° resolution in latitude and longitude, and the vertical resolution is 26 hybrid sigma/pressure levels. The atmospheric model uses CAM4 physics, and the model SST is prescribed. Specifics of the physical components in the model and the experimental designs for this study were described in Part I. Figure 1 shows the three surface boundary configurations used in the aquaplanet, land, and orography experiments, respectively. It should be noted that the idealized Eurasian continent also contains most of the North African continent in the Northern Hemisphere.

In these experiments, the SST distributions are derived from the Qobs described in Neale and Hoskins (2000) and modified in a manner similar to that in Brayshaw et al. (2008). These modifications are necessary to align the SST better with the observed Northern Hemisphere SST distribution during boreal spring. After these modifications (detailed in Part I), the global zonally symmetric SST is described by

$$\mathrm{SST}(\phi) = \frac{T_{\max}}{2}\left[2 - \sin^4\left(\frac{18\phi}{13}\right) - \sin^2\left(\frac{18\phi}{13}\right)\right], \qquad (1)$$

where $T_{\max}$ is the maximum temperature (set to be 28°C) along the equator, and ϕ is the latitude. The SST calculated from (1) becomes zero at 62.5° latitude, 2.5° closer to the pole than the SST distribution in Brayshaw et al. (2008, 2009). Poleward of 62.5° latitude, SST is set to be 0°C.

For the SST variation representing the AMO, we impose the following monopole SST anomaly on (1):

$$\Delta\mathrm{SST}(\phi,\lambda) = \Delta T_{\max}\cos\left[\pi\left(\frac{\lambda-\lambda_0}{\Delta\lambda}\right)\right]\cos^2\left[\left(\frac{\phi-\phi_0}{\Delta\phi}\right)\right]. \qquad (2)$$

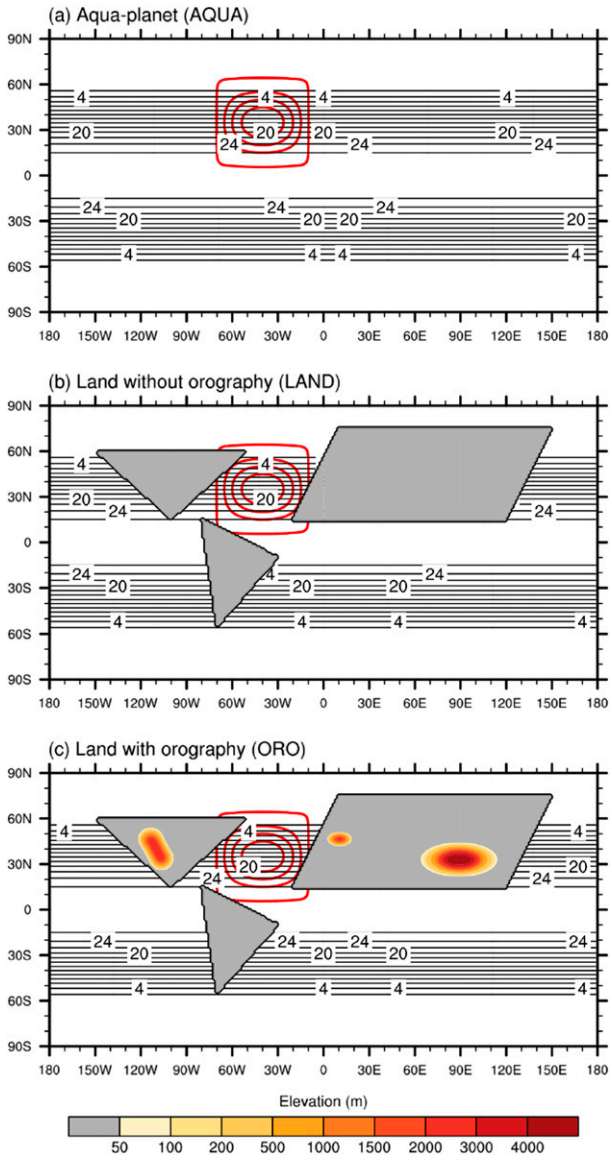

FIG. 1. SST (contour lines) and topography (land and orography in shading) distributions for (a) aquaplanet, (b) land without orography, and (c) land with orography experiments. Concentric circles in the North Atlantic latitude and longitude indicate the location and intensity of the SST anomalies in the warm and cold SST anomaly runs. They are built into the background SST distribution in those experiments. The SST anomaly is 0°C at the outmost contour line and increases or decreases by 1°C magnitude to ±4°C at the center.

In (2), $\Delta T_{\max}$ is the maximum anomaly (±4°C); λ, λ_o, and $\Delta\lambda$ are the longitude, longitude at the center, and longitudinal radius of the SST anomaly, respectively; and ϕ, ϕ_0, and $\Delta\phi$ are the same for the SST anomaly but in latitude. The SST anomaly is centered at 32.5°N and 40°W, with a 30° radius in both latitude and longitude, shown in Fig. 1a by the concentric circles.

As discussed in Part I, the maximum SST anomaly of ±4°C used in (2) is greater than the observed SST anomalies in the AMO (0.5°–1.0°C). Because the only forcing for each set of the experiments is the SST variation, such an enlarged amplitude of the SST variation can increase the signal-to-noise ratio in the responses. The same idea has been used in several previous studies of a similar nature [e.g., ±3°C for SST anomaly in Brayshaw et al. (2008, 2011), 5°C in Webster (1981), and 2.5° and 5°C in Ting and Held (1990)]. Nonetheless, caution should be taken in interpreting the outcomes of the model runs to focus on the patterns in the response.

The shape of the SST anomaly region is determined based on the following. The warm or cold SST phase of the AMO is featured with basinwide positive or negative SST anomalies in the North Atlantic Ocean, although there is a strong anomaly center around 45°N and 45°W (Enfield et al. 2001). To represent this basinwide SST anomaly feature and also simplify the problem so as to allow clear interpretations of model results, we smooth out the anomaly center in the middle latitude and arrive at the SST anomaly described in (2). It is necessary to point out that the basinwide SST anomaly pattern in (2) is rather different from the North Atlantic Drift (in the region 50°–64°N and 10°–30°W) examined in Brayshaw et al. (2011).

To gain understanding of the SST effect in the AMO on North American precipitation and also to explore the mechanism of the AMO-related SST forcing on atmospheric circulation described in Part I, we examine the variation in the eddy kinetic energy (EKE) involved in the middle-latitude storm tracks and precipitation systems (Lau 1978, 1979; Kaspi and Schneider 2011a,b). Following Kaspi and Schneider (2011a), we calculate the vertically integrated EKE from $\mathrm{EKE} = \int_{p_s}^{p_T} [(u')^2 + (v')^2]\, dp/(2g)$, where u' and v' are bandpass-filtered zonal and meridional wind speed, respectively; g is the gravitational acceleration; and p_s and p_T are the atmospheric pressure at the surface and the top model level, respectively.

In a baroclinic environment, such as the circulation induced by North Atlantic basinwide SST anomaly, baroclinic eddies develop to convert potential energy to kinetic energy. They transport, release, and mix heat between the low and mid-to-high latitude, in the form of weather systems of various scales, consuming the baroclinicity. Because of the rotation of Earth, the heat release and mixing by the baroclinic eddies is concentrated in certain regions along the middle latitude, where storm tracks form (Kaspi and Schneider 2011a). These storm tracks are distinctive over the oceans. Upstream in the land areas (i.e., North America), the eddy activities are primarily organized by quasi-stationary Rossby waves excited by the SST anomalies in the ocean (e.g., Kaspi

and Schneider 2011b). Dependent on the nature of the SST forcing (e.g., warm versus cold SST anomaly), the eddy activities over the continents will differ and result in different responses in storms and precipitation.

Following this line of thought, we analyze the anomalies in circulation and embedded eddy activities in terms of EKE, in response to the warm and cold SST anomaly in the AMO. From these analyses, we may quantify distinct, or intrinsic, effects of the AMO on North American precipitation.

In addition to the above analyses, we also examine the maximum Eady growth rate variation (Charney 1947; Eady 1949; Keyser and Anthes 1982; Hoskins and Valdes 1990). This growth rate is measured by $\sigma = 0.31f|\partial \mathbf{V}/\partial z|N^{-1}$, where f is the Coriolis parameter, $\mathbf{V}$ the wind velocity, z the geopotential height, and N the Brunt–Väisälä frequency. This frequency is defined, after a slight alteration of that in Keyser and Anthes (1982), as $N = [(g/\theta_0)(\partial\Theta/\partial z)]^{1/2}$, where Θ is the potential temperature and θ_0 is the reference potential temperature at 1000 hPa. This growth rate contains the information of baroclinicity (in the numerator) and buoyancy or convective stability (in the denominator) and measures their collective effect on potential for development of weather systems. Because of such a property, Eady growth rate remains large on the equatorward side of 30° latitude [to about 15° latitude before f is too small (see Brayshaw et al. 2008, 2011)], where it can provide a measure for the stability of the atmosphere. In our analysis, the partial derivatives in σ are calculated in finite differences between 925 and 250 hPa.

3. Results

a. *Major features in circulation response to the SST anomaly*

We first show in Fig. 2 the mean upper-troposphere zonal winds for March derived from the 1981–2010 climatology of the NCEP–NCAR Reanalysis data (Kalnay et al. 1996) and the zonal winds from the model equilibrium solutions for the three sets of experiments (i.e., aquaplanet, land, and orography) without an SST anomaly (their control runs). The winds from the aquaplanet (Fig. 2b) show an axisymmetric pattern of easterly flows in the tropics and at the pole and westerly flows in between. The strongest westerly is in the single subtropical jet [similar to Fig. 2a in Brayshaw et al. (2011)]. These zonal wind fields will be used later in discussions of the relevance of the orography experiment to the real world and the implications of its results.

After the SST anomalies are introduced in the experiments, the wind and mass fields change. These changes are measured by the difference (anomaly) from the control run solution. The geopotential and wind anomalies in response to the SST anomalies in the North Atlantic were discussed in Part I and are briefly summarized here for continuity and reference.

Warm SST anomalies in the North Atlantic Ocean cause an increase in atmospheric convection and precipitation over the warm SST region (Fig. 3a in Part I). Diabatic heating due to convection expands the atmospheric column vertically, resulting in lower pressure in the lower troposphere and higher pressure aloft. In the lower troposphere, air parcels north of the warm SST region would converge to the low pressure region, reducing their planetary vorticity. In our idealized experiments, this change is compensated by increase in relative vorticity of the parcels to conserve their potential vorticity. The increasing relative vorticity in the warm SST region will enhance the low pressure around and also on the west side of the warm SST center, initiating Rossby waves. Associated with these waves are a strong anomalous northerly flow on the west of the warm SST center and a southerly flow on the east. With a single heating over the North Atlantic, the wavenumber-1 Rossby wave will have a ridge west of the strong northerly flow in most of the North American continent and a trough stretching from the warm SST center downstream across most of the Eurasian continent.

This wave pattern of the atmospheric mass and wind in response to the warm SST anomaly in the North Atlantic is shown in our results reported in Part I and reproduced in Figs. 3a–c for the lower troposphere. It is important to note that these results are not the linear responses to a specified background flow/basic state, as in the way often used in examining stability of a basic flow to specific disturbances. These results are equilibrium solutions of the circulation and precipitation under the specified lower and upper (solar insolation at the spring equinox) boundary conditions.

Figures 3a–c show a similar anomaly pattern among the three experiments of aquaplanet, land, and orography, with a ridge or positive geopotential height anomaly upstream and a trough or negative geopotential anomaly downstream of the warm SST region in the North Atlantic. This pattern is also similar to that from idealized experiments in Kaspi and Schneider (2011b; see their Fig. 2d). It dictates a strong anomalous anticyclonic circulation in the lower troposphere over North America and an anomalous cyclonic circulation in most of the Eurasian continent, except in the Far East and the subtropics.

The circulation responses to the cold SST anomaly (Figs. 3d–f) show, on average, negative geopotential

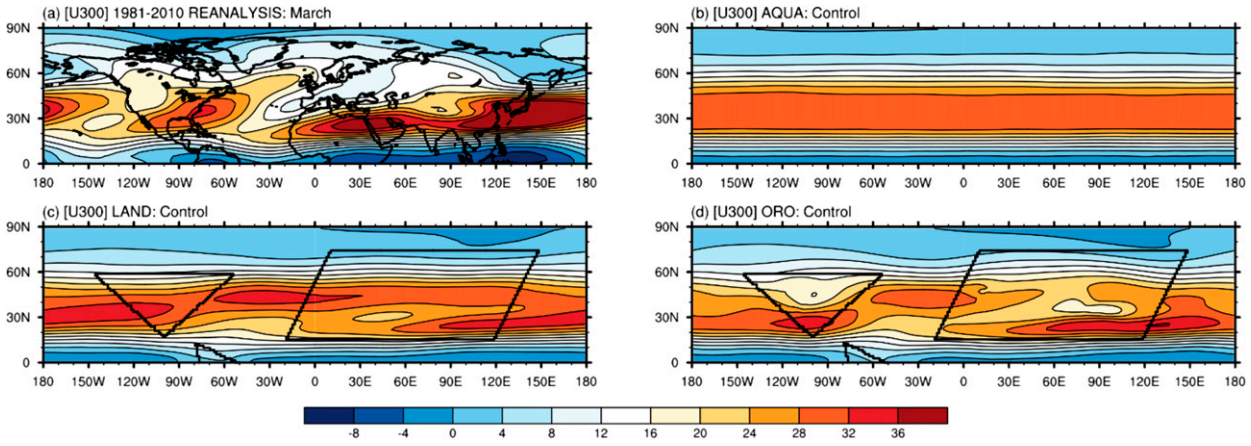

FIG. 2. (a) Mean 300-hPa zonal winds for March, derived from the NCEP–NCAR Reanalysis data (1981–2010). Zonal winds of the model equilibrium solutions from the (b) aquaplanet, (c) land, and (d) orography experiment without SST anomaly (control run).

height anomalies upstream and positive anomalies downstream of the cold SST region, They are nearly an inverse or a mirror image of that to the warm SST anomaly, although the centers of the negative geopotential anomaly over North America change considerably in both their location and intensity between the three experiments. Such changes suggest a sensitivity of the response to other potentially concurring forces during the cold SST anomaly, as discussed in Part I and further elaborated in section 3d. There are southerly winds in the west of the cold SST center and northerly winds in the east. This anomaly pattern dictates an anomalous cyclonic circulation over North America and an anomalous anticyclonic circulation in most of the Eurasian continent in response to the cold SST anomaly in the North Atlantic.

b. EKE and precipitation responses to a warm SST anomaly in the experiments

These anomalous circulations in response to the SST anomalies create regions favorable or unfavorable for eddy activities, storm development, and precipitation. The vertically integrated EKE for eddies of a 2–6-day period range for the aquaplanet, land, and orography experiments is shown in Fig. 4. Figures 4a–c show the EKE response to a warm SST anomaly. In the aquaplanet (Fig. 4a), the EKE anomaly shows enhanced transient eddy activities from the northeast quadrant of the warm SST region in the North Atlantic extending downstream with a slight northeastward orientation to the date line. West of the warm SST center are suppressed activities for those eddies in latitudes from 20°–55°N. These transient eddy activities are similar to that in Kaspi and Schneider (2011b; see their Fig. 2a). They are also consistent with the cyclonic circulation anomalies downstream of the warm SST center and anticyclonic circulation anomalies upstream (Fig. 3a). The most intense eddy activity, shown by the largest positive EKE anomaly, is found immediately downstream of the warm SST center, where the southerly winds in the trough (Fig. 3a) have strong positive relative vorticity (elaborated in Part I). West and upstream of the warm SST center, the weak negative EKE anomaly indicates suppressed eddy activity, consistent with anticyclonic circulation and negative relative vorticity in that region.

Anomaly patterns similar to the above from the aquaplanet run are found in the results from the land and also the orography experiments, shown in Figs. 4b and 4c, respectively. While there are minor differences in these results compared to Fig. 4a, owing to additional baroclinicity rising from the uneven heating across the land and orography (Part I), the overall EKE anomaly pattern shows enhanced transient eddy activity from the northeast of the warm SST region stretching downstream across the northern half of the Eurasian continent. Meanwhile, suppressed EKE is shown extending from the warm SST region upstream across most North America and farther into the North Pacific Ocean, where an anticyclonic circulation anomaly is dominant in response to the warm SST anomaly in the North Atlantic (Fig. 3b).

The transient eddy activities measured by the EKE anomaly in Figs. 4a–c explain large portions of the precipitation anomalies in the middle and high latitudes in response to the warm SST anomaly (shown in Figs. 5a–c). However, we notice that in the subtropics and inside the warm SST anomaly region, positive/negative anomalies in EKE do not always correspond to the same anomalies in precipitation. These differences indicate that processes other than the transient eddies are strongly influencing the precipitation in those regions.

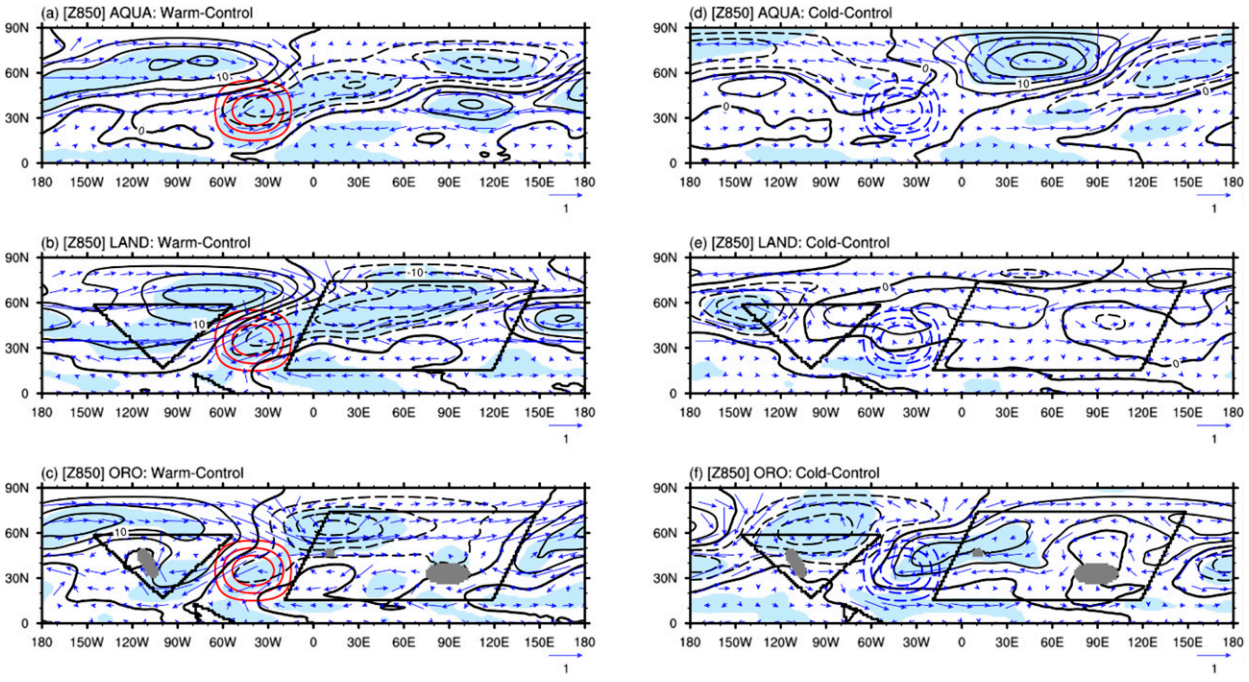

FIG. 3. Anomalies of geopotential height (m; contour lines; contour interval: 5 m) and winds (m s^{-1}; arrows) at 850 hPa from aquaplanet, land, and orography experiments (taken from Part I). (a)–(c) Responses to warm SST anomaly; (d)–(f) responses to cold SST anomalies. Data are filtered using a two-dimensional Gaussian filter with a standard deviation of 4.2°. Shading indicates changes are significant at the 95% confidence level. Warm (red) and cold (blue) SST anomalies are shown in concentric circles.

For example, inside the warm SST region, strong convection (as shown by large rate of latent heating in Fig. 3a of Part I) is dominant and results in the strong positive precipitation anomaly shown in Fig. 5a. Outside the warm SST region and in the subtropics and tropics, convection and large-scale (meridional) circulation play important roles in precipitation development while transporting energy poleward. Transient eddy processes on the synoptic scale are less active, or absent, equatorward of 30° latitude than in the midlatitude in both hemispheres (e.g., Oort 1971).

The strong effects of convection and mean circulation in low latitudes are partially suggested by the maximum Eady growth rate, shown in Fig. 6a for the aquaplanet experiment. An indication is shown in the region upstream of the warm SST center between 20° and 30°N latitude. This region extends westward around the globe with separate centers of positive growth rate. It suggests strong convection that could explain part of the positive anomalies in precipitation across those subtropical latitudes (Fig. 5a).

The response of precipitation in the land experiment (Fig. 5b) is found to be similar to that in the aquaplanet experiment, particularly upstream of the warm SST anomaly center. In most of midlatitude North America (30°–55°N), (statistically) significant negative anomalies in precipitation are found in areas with suppressed EKE (Figs. 5b and 4b) under a positive geopotential anomaly (ridge in upstream of the warm SST center; Fig. 3b). Both poleward and equatorward of this zone of suppressed rainfall are positive anomalies in precipitation. The increase in precipitation in the north is supported by positive EKE. The positive precipitation anomaly in the subtropics is, however, unlikely to be fully explained by anomalies in the maximum Eady growth rate (Fig. 6b). Although Fig. 6b shows a small area in the subtropical North Pacific (around the date line) with weak positive Eady growth rate, it is insufficient to account for the strong positive precipitation anomaly in the broad region from 30°N to the equator (Fig. 5b) upstream of the warm SST anomaly center. In the tropical and subtropical latitudes, where the synoptic eddies are weak or absent (Fig. 4), large-scale circulation organizes atmospheric moisture and produces convection and precipitation. Anomalies in such circulations in response to the SST anomaly can contribute to precipitation variations.

To show this effect, we computed the column-integrated large-scale moisture divergence response to the SST anomaly in the North Atlantic. The results are shown in Figs. 7a–c for the warm SST anomaly. Figure 7b clearly shows strong convergence of moisture

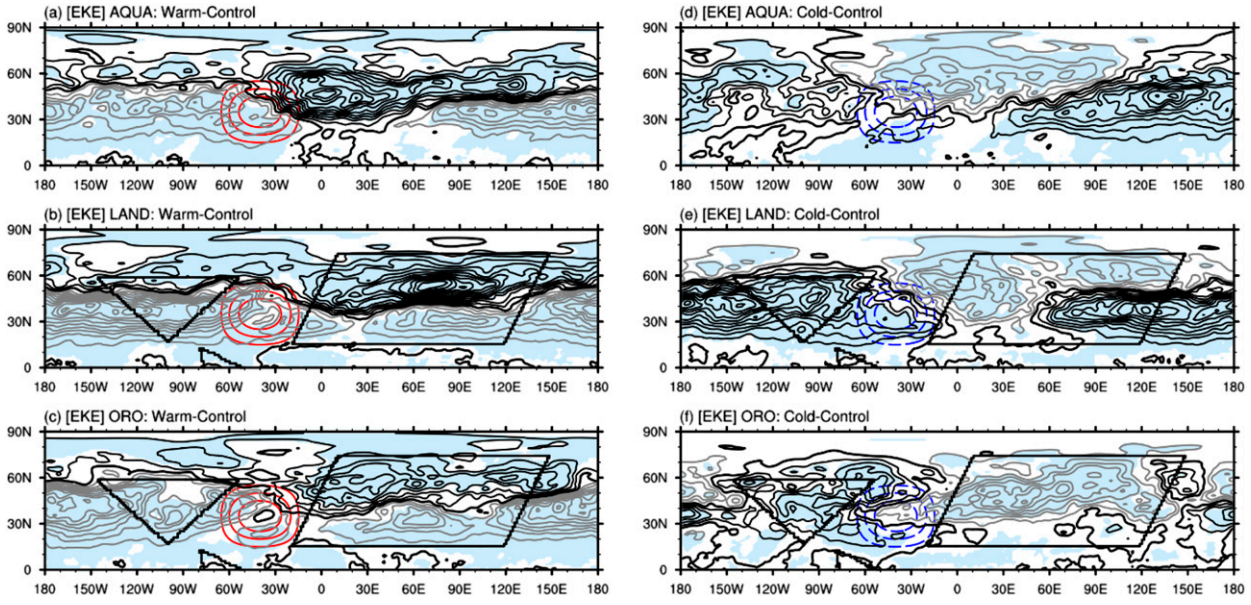

FIG. 4. Vertically integrated bandpass-filtered EKE anomaly (MJ m^{-2}; contour interval: 0.005 MJ m^{-2}) for eddies of the 2–6-day period range in response to (a)–(c) warm and (d)–(f) cold SST anomaly in the aquaplanet, land, and orography experiments. Dark lines are for positive anomalies, and gray lines are for negative anomalies. Data are filtered using a two-dimensional Gaussian filter with a standard deviation of 4.2°. Shading indicates changes from the control run are significant at the 95% confidence level.

in the atmospheric column in the broad region from 30°N to near the equator upstream of the SST anomaly center, where positive precipitation anomalies occur. While this region of moisture convergence is pierced by some divergence in the south and southwest of the idealized North America, the convergence in the southeast of the continent contributes to the positive precipitation anomaly around the south tip of the continent.

South of the warm SST anomaly center and also downstream along the equator, strong anomalies in

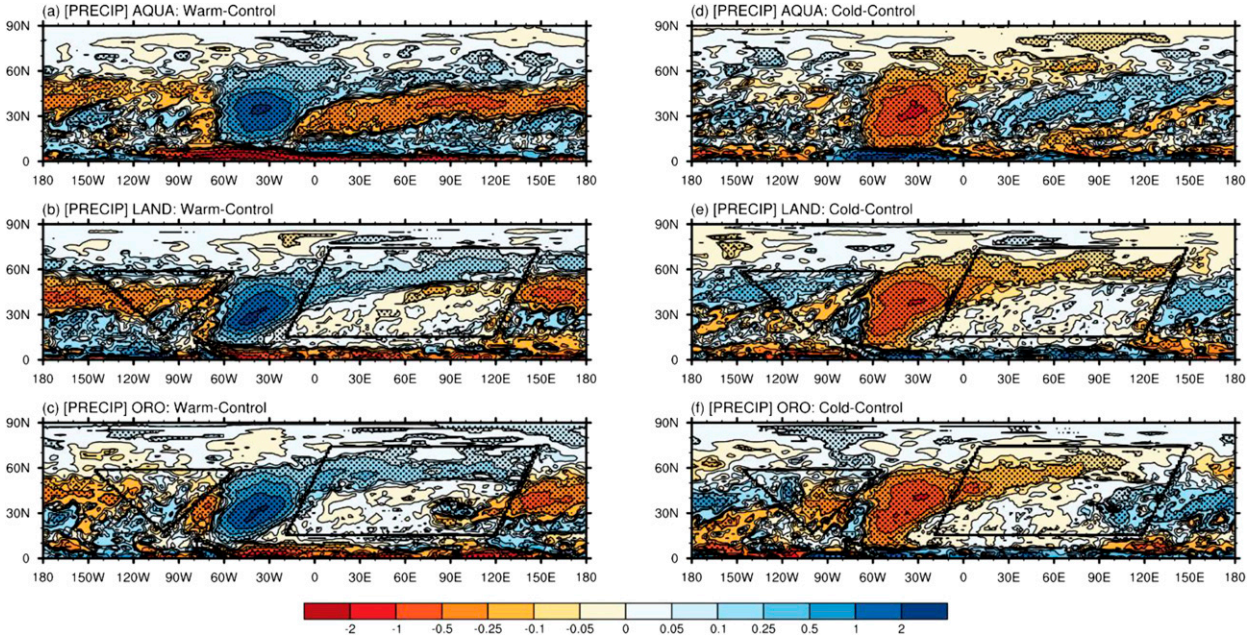

FIG. 5. Precipitation anomaly (mm day^{-1}) in response to (a)–(c) warm and (d)–(f) cold SST anomaly in the aquaplanet, land, and orography experiments. (Data are not filtered.) Stippled areas have significant variations in precipitation from the control run at the 95% confidence level based on a two-tailed Student's *t* test.

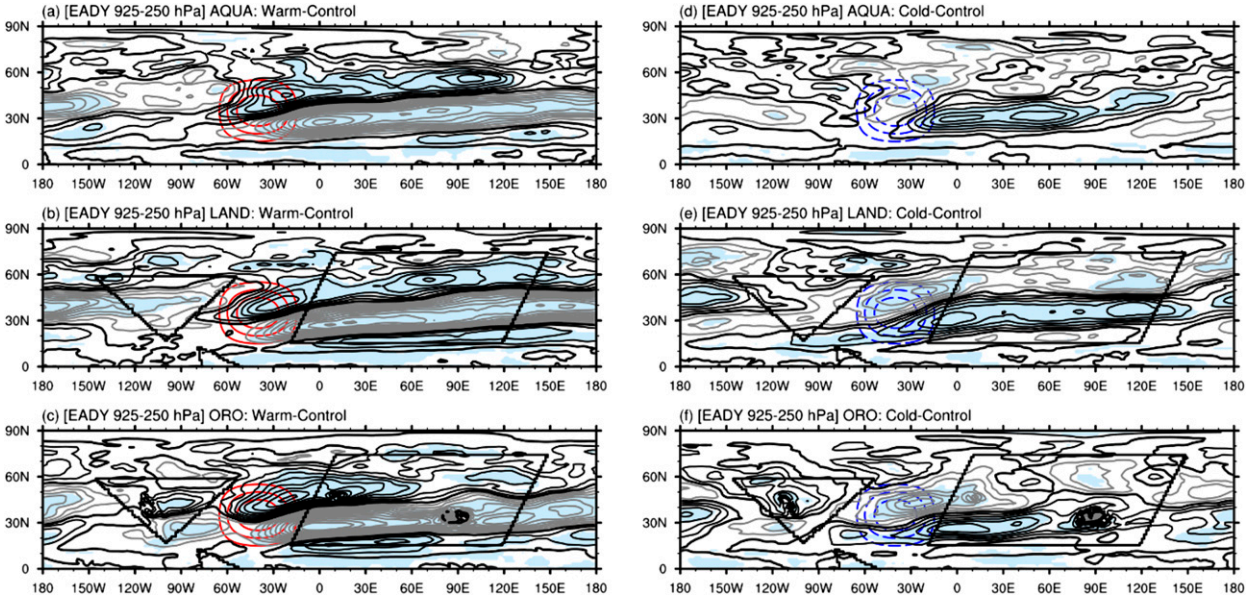

FIG. 6. Anomaly in maximum Eady growth rate (s^{-1}; contour interval: $10^{-7}\,s^{-1}$) in response to (a)–(c) warm and (d)–(f) cold SST anomaly in the aquaplanet, land, and orography experiments. Data are filtered using a two-dimensional Gaussian filter with a standard deviation of 4.2°. Dark lines are for positive anomalies, and gray lines are for negative anomalies. Shading indicates changes from the control run are significant at the 95% confidence level.

moisture divergence largely explain the deficit in precipitation (cf. Figs. 7b and 5b). North of the equator, weak moisture divergence across the subtropics of the Eurasian continent is consistent with reduced precipitation. In the midlatitude of that continent, a positive precipitation anomaly is associated with a high positive EKE anomaly and also moisture convergence inside the trough (Fig. 3b).

When major orography is included in the idealized continents the mountains and plateau add their strong signatures in meridional energy, as well as moisture transport in the atmosphere and subsequent changes in storm tracks and precipitation, in response to the warm SST anomaly. Figures 3c, 4c, and 5c show those responses. Compared to Fig. 5b from the land experiment, Fig. 5c shows a less organized precipitation anomaly, particularly in the leeward of the Rocky Mountains in idealized North America, where the response is tested to be statistically insignificant (at the 95% confidence level). [Similar changes are also shown in Brayshaw et al. (2011).] This change is consistent with the weakened EKE anomaly (Fig. 4c), although an increase in moisture convergence in that region (Fig. 7c) allows for more precipitation (compared to the land experiment result in Fig. 5b). This increase in moisture convergence in that region could be a combined result of increasing northward transport of moisture and enhanced southerly flow along the west fringe of the established North Atlantic subtropical high in the orography experiment (see Part I for details of the processes). In the windward and north of the Rockies in North America, moisture divergence (Fig. 7c) with suppressed EKE (Fig. 4c) sustain a significant negative anomaly in precipitation.

Because the orography experiment is closest to the real-world condition, its precipitation response to the SST anomaly should share some basic characteristics of the response in the real world. With this similarity, the precipitation response in Fig. 5c (and later Fig. 5f for response to a cold SST anomaly) could help disclose the intrinsic effect of the SST variation in the AMO on North American precipitation. It is important to note, however, as previously cautioned, that we only focus on the signs and spatial variations in the precipitation response, not on its magnitudes. To examine such representativeness, we compare the zonal winds at 300 hPa from the control run of the orography experiment (Fig. 2d) and the mean zonal winds for March derived from the NCEP–NCAR Reanalysis data (Fig. 2a). In Fig. 2a, a streak of strong zonal winds extends from subtropical North Africa (20°–25°N) through the South Asian continent to the eastern North Pacific before reaching North America. Over North America, a core of strong zonal winds stretches from the eastern North Pacific, but at a latitude south of the exit of the previous jet, across the south of North America to the midlatitude North Atlantic Ocean.

The model solution in Fig. 2d from the orography run shows a similar streak of strong zonal winds through

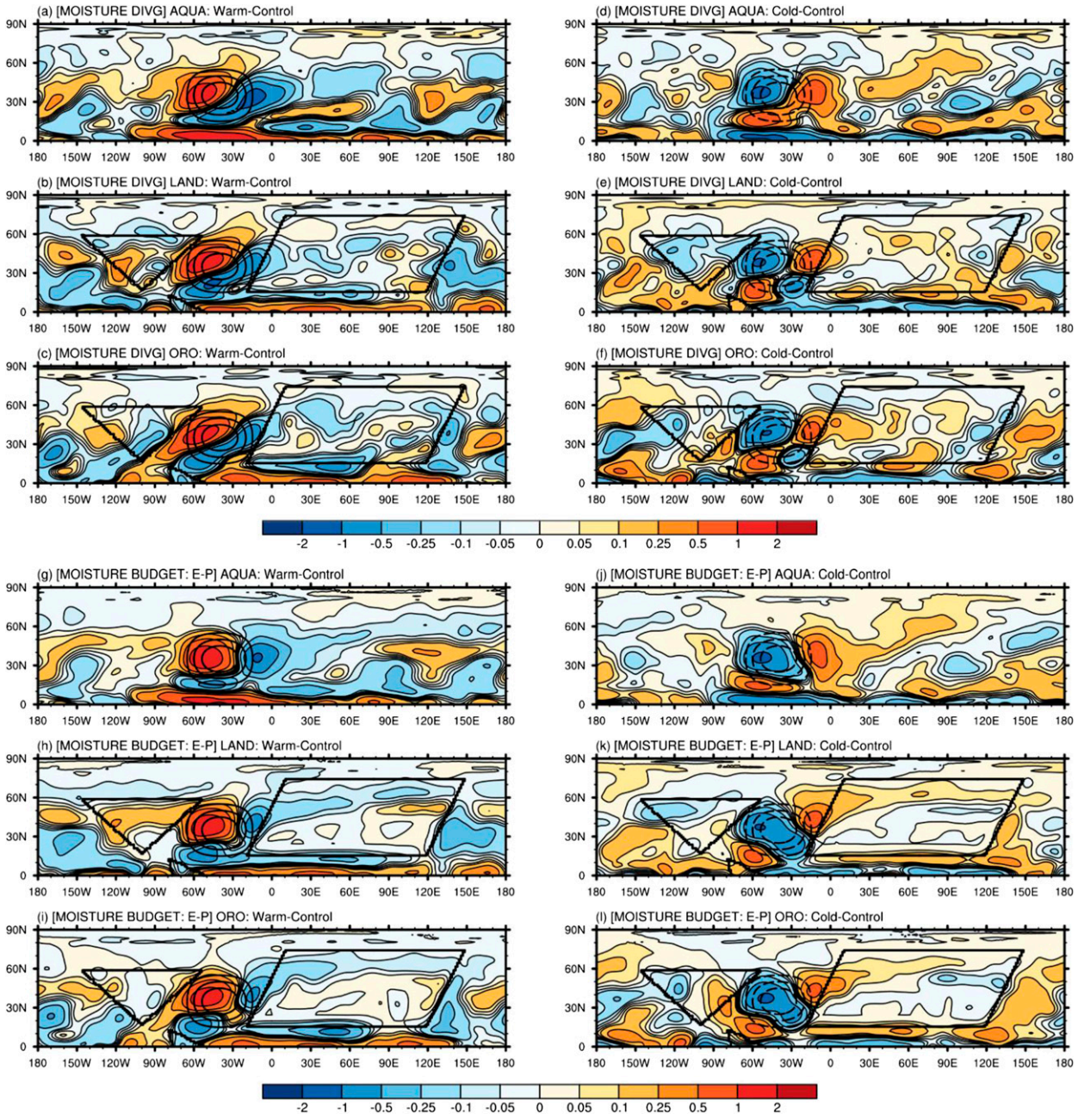

FIG. 7. Response of vertically integrated moisture divergence anomaly (mm day^{-1}) to a warm SST in the (a) aquaplanet, (b) land, and (c) orography experiment. (d)–(f) As in (a)–(c), but in response to the cold SST anomaly. The anomalies of vertically integrated moisture divergence/convergence can be comprehended with the following results: (g)–(l) as in (a)–(f), but in response to the anomaly of evaporation (E) minus precipitation (P) at the surface. Data are filtered using a two-dimensional Gaussian filter with a standard deviation of 4.2°.

the idealized south Eurasian continent, although the strength of the winds in the eastern North Pacific is weaker than the observed, and the streak is also narrower. The latitude of this jet is also southward by about 5° from the observed. Also similar is a separate core of strong zonal winds extending across the south of the idealized North America into the midlatitude North Atlantic Ocean. Again, the latitude of this jet is south from the observed. These differences in latitude of the jet cores and the lack of a northward tilt of the jet crossing the Eurasian continent (into the northeast North Pacific) could be attributed to the smaller size of the idealized continents, especially in the high latitudes, and also the specified 0°C for SST north of 62.5°N, which

is warmer than the observed surface condition in March in the polar region. Although these differences/biases result in differences in the simulated mean circulation, storm tracks, and precipitation from the observed, the similarity of the jet streams and their positions relative to the continents between the idealized orography world in the model and the observed suggests that the control run of the orography experiment has captured the basic characteristics of the circulation and storm track relative to the continents.

With this similarity, we would postulate that the results from the orography experiment have relevant representativeness for major characteristics in the precipitation response to the SST variations during the AMO. With this representativeness, we can conclude, based on the previously discussed results, that the warm SST anomaly in the North Atlantic Ocean during the AMO would cause suppressed precipitation in most of central and northwest North America and more precipitation in its southeast.

c. *Precipitation responses to a cold SST anomaly in the experiments*

The precipitation response to a cold SST anomaly in the North Atlantic is nearly a reverse of that to the warm SST anomaly in all three experiments (Fig. 5), although the details differ considerably. In the aquaplanet (cf. Figs. 5d and 5a), we notice that the precipitation anomalies both upstream and downstream in response to the cold SST anomaly are less organized than the response to the warm SST (Fig. 5a). In detail, there is suppressed precipitation over the cold SST region and in the downstream high-latitude region (Fig. 5d), where positive geopotential anomalies developed (Fig. 3d). In most of the midlatitude region downstream of the cold SST, there are positive anomalies in precipitation. Upstream of the cold SST region, while there are more positive anomalies in precipitation on average, consistent with the negative geopotential anomaly, they are mixed with small areas of negative anomaly. This mix makes the response statistically insignificant (at the 95% confidence level) in most of the upstream region.

An averaged increase in precipitation upstream of the cold SST anomaly center (cf. Figs. 5d and 5a) is supported by broad positive EKE anomalies in the upstream region (Fig. 4d), where a mix of divergence and convergence of moisture with weak amplitude is also seen (Fig. 7d). Consistently, the suppressed precipitation downstream of the cold SST anomaly center is associated with suppressed EKE and negative maximum Eady growth rate in the enhanced ridge area from the north of the cold SST center to about 120°E, before becoming positive again in the area east and south of the ridge. There is also strong moisture divergence downstream in the enhanced ridge area and convergence in its south and east (Fig. 7d).

In the land experiment, we again find that the continents help to better organize the responses in EKE (Fig. 4e) and the precipitation (Fig. 5e), particularly upstream of the SST anomaly. This can be seen from comparing the results between the land and the aquaplanet experiments in Figs. 4–7.

When orography is added, it increases the meridional variation in the responses, thus weakening the organized strong zonal structure in the response from the land experiment and making the response more varying across the idealized North America (cf. Figs. 4e–7e and Figs. 4f–7f). Such enhanced variations in precipitation are also indicated by statistical tests, which show most of the variations in North America are significant at the 95% confidence level (Fig. 5f).

It is interesting to notice that in the results of the orography run we see positive anomalies in both the EKE and the maximum Eady growth rate in the idealized North America (although the Eady growth rate has negative anomalies in the southern tip and along the eastern fringe of the continent) in response to the cold SST anomaly (Figs. 4f, 6f). Yet we see strongly varying anomalies in precipitation, with positive in the central and west and negative in the south and southeast of the continent (Fig. 5f). The unexplained negative anomaly in precipitation in the south and southeast by the synoptic eddies may be attributed to a lack of sufficient moisture in that region during the cold SST anomaly. As shown in Fig. 7f, there is a spread of moisture divergence by large-scale circulation in the south and southeast in North America. This moisture divergence anomaly undermines convection and precipitation in those areas. This particular set of anomalies in synoptic eddies and the large-scale moisture field suggests the presence of active eddies in North America in response to the cold SST anomaly. Precipitation can result from them when sufficient moisture is available. This dynamically charged condition during the cold SST anomaly makes the precipitation in North America more prone to fluctuations in moisture availability. This result could explain the strong (statistically significant) variation in precipitation in response to the cold SST anomaly discussed earlier and may also provide a reason for the significant interannual fluctuations of the simulated precipitation in North America during the cold phase of the AMO in more realistic models (e.g., Hu et al. 2011).

The results presented so far show strong effects of the SST anomaly in the North Atlantic Ocean on North American precipitation. When they are interwoven with

the results in Part I, which has details in circulation responses, they provide an answer to one of our two questions: the North Atlantic SST anomaly associated with the AMO has a distinct effect on warm season circulation and precipitation in North America; the observed statistical relationship from historical and reanalysis data is describing a physical and dynamic connection.

d. More sensitivity of the response to cold SST anomaly and explanation

The dynamically charged condition in North America discussed earlier during the cold SST anomaly would favor strong temporal variations in precipitation (supported by the statistical test result). In contrast, the more dynamically stable condition (negative anomalies in EKE and maximum Eady growth rate) in response to the warm SST anomaly would favor less varying precipitation in North America (also consistent with more areas of insignificant variation in the test result). These differences could partially explain the question of why the observed precipitation in North America during the warm phase in AMO is more stable in time than in its cold phase. Another possible explanation to this question was suggested in Part I: that is, the circulation response to the cold SST anomaly in the North Atlantic is more sensitive to forcings other than the SST anomaly, such as the land and orography in these experiments (or forcing rising during the cold SST phase). This sensitivity is shown in Part I by dramatic changes in the equilibrium solutions depicting the response of the circulation (the geopotential and winds) to the cold SST anomaly between the three sets of experiments, in contrast to fairly similar or stable responses to the warm SST anomaly in those experiments. These differences show contrasting dynamic characteristics between the equilibrium solutions in North America in response to cold and warm SST anomalies in the North Atlantic. These characteristics define the stability of those equilibrium solutions. As shown, the solution in response to the warm SST is more stable, and the one in response to the cold SST is susceptible/sensitive to moisture and other forcing and is thus more varying or less stable in time (during the course of the cold SST anomaly).

To further elaborate on this sensitivity, we examine the EKE of eddies at different frequencies but within the short-to-medium-range weather process in response to the SST anomaly in the North Atlantic. This attempt is prompted by our results in Fig. 4 showing substantial changes in the EKE of eddies at the 2–6-day range from the land to the orography experiment (Fig. 4f vs Fig. 4e, in contrast to Fig. 4c vs Fig. 4b). Such a change suggests a strong sensitivity of eddies of the 2–6-day period range to the orography, which represents a forcing other than the SST, in those experiments with the same SST anomaly. If eddies of different frequencies have strong and different responses to the forcing under the same SST anomaly, the total effect of the eddies in response to the SST anomaly would suggest a strong sensitivity of the equilibrium state to other forcings that may arise during the cold SST anomaly.

Following this line of thought, we calculated and show in Fig. 8 the anomalies in EKE of transient eddies of the 7–10-day medium range in the three sets of experiments. With a warm SST, Figs. 8a–c show anomalies in the EKE of those eddies consistent with that of eddies of the 2–6-day periods (Figs. 4a–c), albeit the magnitude of the former is smaller. In contrast, comparing the anomalies of the EKE for eddies of 7–10 days against the 2–6-day period range in response to the cold SST anomaly (cf. Figs. 8d–f and Figs. 4d–f), we find quite large differences between the EKE of those eddies upstream of the cold SST center in the aquaplanet and land experiments. It is striking that the EKE response for eddies of the 7–10-day period range is nearly opposite to that of the 2–6-day period range in the orography experiment (cf. Figs. 8f and 4f).

These nearly opposite responses of different eddies suggest that the responses in circulation and precipitation in idealized North America (with orography) are more sensitive to or easily varying because of other forcings during the cold SST anomaly than in the warm SST anomaly. This result supports, from an additional aspect, the more dynamically charged condition in North America in response to the cold SST anomaly in the North Atlantic. Because of such a condition, the responses in circulation (Part I) and precipitation are more varying in response to the cold than to the warm SST anomaly, even though the general pattern would favor more precipitation in central and northwestern North America and suppress precipitation in its south and southeast. Results from these analyses provide an answer to the second question on why the observations have shown more fluctuations in precipitation variation and hence more spatial variation in the precipitation anomaly pattern in North America during the cold phase of the AMO.

4. Summary and concluding remarks

Extending the work in Part I, we have examined precipitation responses in North America to the warm and cold SST anomaly in the North Atlantic Ocean, in the same set of idealized model experiments under the perpetual spring equinox conditions.

Consistent with the atmospheric circulation responses to the warm/cold SST anomaly (detailed in Part I), the

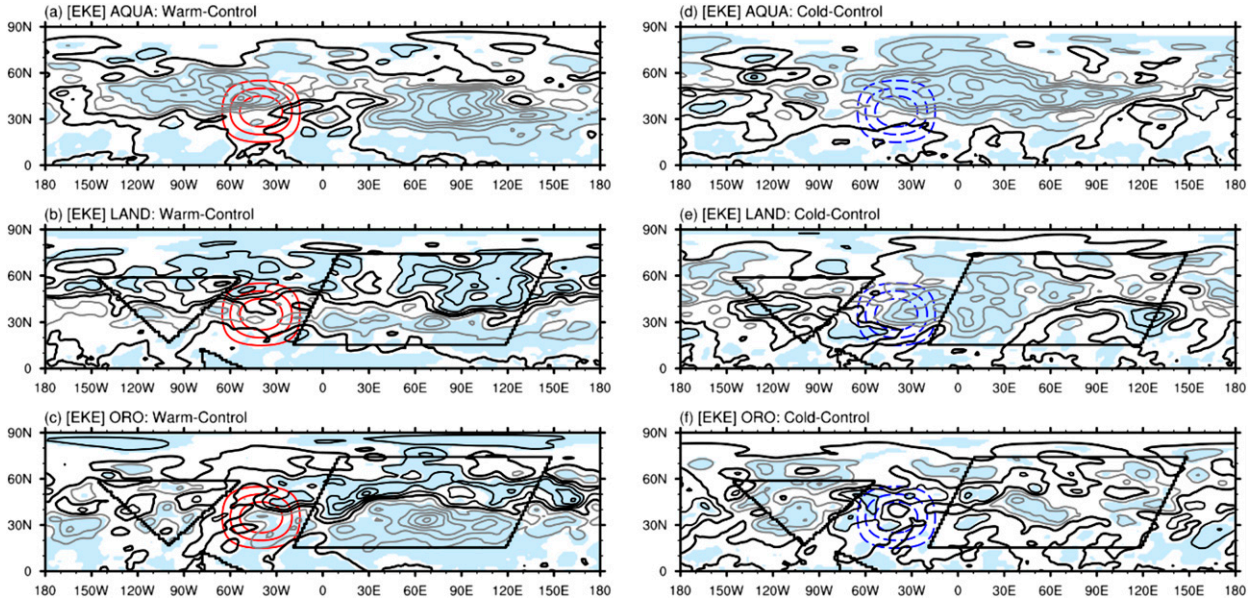

FIG. 8. As in Fig. 4, but for eddies of the 7–10-day period range.

precipitation shows a distinct anomaly pattern in idealized North America in response to the warm/cold SST anomaly in the North Atlantic Ocean. In response to the warm SST anomaly, results from the aquaplanet to the orography experiment (the latter is the closest to the real-world condition) show fairly consistent suppressed precipitation in most of North America except for its south and southeast. These results are coherent with the positive geopotential anomaly in circulation over most of idealized North America in those experiments. Nearly inverse anomaly patterns are shown in both the circulation and precipitation in North America in response to the cold SST anomaly, although details differ substantially. These results derived from the properly designed experiments indicate that the SST anomaly associated with the AMO has a distinct effect on or corresponding anomalies in circulation and precipitation in North America, supporting the observed statistical relationship of the AMO and multidecadal variation in warm season precipitation in North America.

Moreover, in examining the dynamic aspects of the equilibrium solutions (states of the atmospheric circulation and precipitation) in the sets of model experiments, we find that the equilibrium solutions in response to the warm SST anomaly are more stable than the solution in response to the cold SST anomaly. The weak stability in the latter is suggested by two features in the solutions: 1) The equilibrium solution in response to the cold SST anomaly is dynamically charged in the sense that the EKE, as well as the maximum Eady growth rate, indicates favorable conditions for disturbances and precipitation development in most of North America, yet precipitation is suppressed particularly in the southeast and southcentral regions because of a lack of a sufficient moisture supply. In other words, the condition in the response is incoherent between its dynamic and moisture fields. This volatile condition could cause large fluctuations in precipitation in those areas dependent on variations in moisture availability. This potential is further indicated by the statistical test showing significant precipitation variation in the cold SST case, in contrast to the insignificant variation of precipitation in most of the idealized North America in response to the warm SST anomaly. 2) There are rather different responses of transient eddies between short- and medium-range weather frequencies (2–6- and 7–10-day period range, respectively) in the orography experiment. Eddies of the 7–10-day period range respond in North America to the cold SST anomaly in a pattern nearly opposite to that by eddies of the 2–6-day period range. Thus, conditions in which either one of such competing effects is enhanced can result in changes in the responses of the circulation and precipitation in North America to the same cold SST anomaly. These conditions undermining the stability of the response in the cold SST anomaly are not observed in the orography experiment in response to the warm SST anomaly. This difference may further raise the potential for a more varying pattern/anomaly in warm season precipitation in North America during the cold than the warm SST anomaly in the North Atlantic, as indicated in the observations (e.g., Hu and Feng 2008; Wang et al. 2010; Nigam et al. 2011) as well as in more realistic GCM simulations (e.g., Hu et al. 2011).

An implication of these results is that predictions of multidecadal variation in regional precipitation may be improved only when both the distinct effects of SST anomalies, such as the AMO, PDO, and ENSO, and their modifications by processes that may become active in specific situations during the SST anomaly [such as the moisture flux from the region of the Gulf of Mexico during the warm phase of the AMO (e.g., Wang et al. 2010)] are known and correctly integrated.

Acknowledgments. We thank three anonymous reviewers and the editor for their suggestions and comments that helped improve this work. We are grateful for the financial support from the NOAA Grant NA09OAR4310188 and NSF Grant AGS-1103316 to the University of Nebraska–Lincoln and from the USDA Cooperative Research Project NEB-38-088. The simulations in this work were made using the Yellowstone computing system of the National Center for Atmospheric Research (http://n2t.net/ark:/85065/d7wd3xhc), which is supported by the National Science Foundation.

REFERENCES

Brayshaw, D. J., B. Hoskins, and M. Blackburn, 2008: The storm-track response to idealized SST perturbations in an aqua-planet GCM. *J. Atmos. Sci.*, **65**, 2842–2860, doi:10.1175/2008JAS2657.1.

——, ——, and ——, 2009: The basic ingredients of the North Atlantic storm track. Part I: Land–sea contrast and orography. *J. Atmos. Sci.*, **66**, 2539–2558, doi:10.1175/2009JAS3078.1.

——, ——, and ——, 2011: The basic ingredients of the North Atlantic storm track. Part II: Sea surface temperatures. *J. Atmos. Sci.*, **68**, 1784–1805, doi:10.1175/2011JAS3674.1.

Charney, J. G., 1947: The dynamics of long waves in a baroclinic westerly current. *J. Meteor.*, **4**, 136–162, doi:10.1175/1520-0469(1947)004<0136:TDOLWI>2.0.CO;2.

Eady, E., 1949: Long waves and cyclone waves. *Tellus*, **1A**, 33–52, doi:10.1111/j.2153-3490.1949.tb01265.x.

Enfield, D. B., A. M. Mestas-Nuñez, and P. J. Trimble, 2001: The Atlantic multidecadal oscillation and its relation to rainfall and river flows in the continental U.S. *Geophys. Res. Lett.*, **28**, 2077–2080, doi:10.1029/2000GL012745.

Hoskins, B. J., and P. J. Valdes, 1990: On the existence of storm-tracks. *J. Atmos. Sci.*, **47**, 1854–1864, doi:10.1175/1520-0469(1990)047<1854:OTEOST>2.0.CO;2.

Hu, Q., and S. Feng, 2008: Variation of the North American summer monsoon regimes and the Atlantic multidecadal oscillation. *J. Climate*, **21**, 2371–2383, doi:10.1175/2007JCLI2005.1.

——, ——, and R. Oglesby, 2011: Variations in North American summer precipitation driven by the Atlantic multidecadal oscillation. *J. Climate*, **24**, 5555–5570, doi:10.1175/2011JCLI4060.1.

Kalnay, E., and Coauthors, 1996: The NCEP/NCAR 40-Year Reanalysis Project. *Bull. Amer. Meteor. Soc.*, **77**, 437–471, doi:10.1175/1520-0477(1996)077<0437:TNYRP>2.0.CO;2.

Kaspi, Y., and T. Schneider, 2011a: Downstream self-destruction of storm tracks. *J. Atmos. Sci.*, **68**, 2459–2464, doi:10.1175/JAS-D-10-05002.1.

——, and ——, 2011b: Winter cold of eastern continental boundaries induced by warm ocean waters. *Nature*, **471**, 621–625, doi:10.1038/nature09924.

Keyser, D., and R. A. Anthes, 1982: An alternative expression for the Eady wave growth rate. *J. Atmos. Sci.*, **39**, 1877–1881, doi:10.1175/1520-0469(1982)039<1877:AAEFTE>2.0.CO;2.

Lau, N.-C., 1978: On the three-dimensional structure of the observed transient eddy statistics of the Northern Hemisphere wintertime circulation. *J. Atmos. Sci.*, **35**, 1900–1923, doi:10.1175/1520-0469(1978)035<1900:OTTDSO>2.0.CO;2.

——, 1979: The structure and energetics of transient disturbances in the Northern Hemisphere wintertime circulation. *J. Atmos. Sci.*, **36**, 982–995, doi:10.1175/1520-0469(1979)036<0982:TSAEOT>2.0.CO;2.

Mo, K. C., J. E. Schemm, and S.-H. Yoo, 2009: Influence of ENSO and the Atlantic multidecadal oscillation on drought over the United States. *J. Climate*, **22**, 5962–5982, doi:10.1175/2009JCLI2966.1.

Neale, R. B., and B. J. Hoskins, 2000: A standard test for AGCMs including their physical parameterizations: I: The proposal. *Atmos. Sci. Lett.*, **1**, 101–107, doi:10.1006/asle.2000.0019.

Nigam, S., B. Guan, and A. Ruiz-Barradas, 2011: Key role of the Atlantic multidecadal oscillation in 20th century drought and wet periods over the Great Plains. *Geophys. Res. Lett.*, **38**, L16713, doi:10.1029/2011GL048650.

Oort, A. H., 1971: The observed annual cycle in the meridional transport of atmospheric energy. *J. Atmos. Sci.*, **28**, 325–339, doi:10.1175/1520-0469(1971)028<0325:TOACIT>2.0.CO;2.

Schubert, S., and Coauthors, 2009: A U.S. CLIVAR project to assess and compare the responses of global climate models to drought-related SST forcing patterns: Overview and results. *J. Climate*, **22**, 5251–5272, doi:10.1175/2009JCLI3060.1.

Sutton, R. T., and D. L. R. Hodson, 2005: Atlantic Ocean forcing of North American and European summer climate. *Science*, **309**, 115–118, doi:10.1126/science.1109496.

——, and ——, 2007: Climate response to basin-scale warming and cooling of the North Atlantic Ocean. *J. Climate*, **20**, 891–907, doi:10.1175/JCLI4038.1.

Ting, M., and I. M. Held, 1990: The stationary wave response to a tropical SST anomaly in an idealized GCM. *J. Atmos. Sci.*, **47**, 2546–2566, doi:10.1175/1520-0469(1990)047<2546:TSWRTA>2.0.CO;2.

Veres, M. C., and Q. Hu, 2015: Atmospheric responses to North Atlantic SST anomalies in idealized experiments. Part I: Northern Hemispheric circulation. *J. Climate*, **28**, 6204–6220, doi:10.1175/JCLI-D-14-00413.1.

Wang, H., S. Schubert, M. Suarez, and R. Koster, 2010: The physical mechanisms by which the leading patterns of SST variability impact U.S. precipitation. *J. Climate*, **23**, 1815–1836, doi:10.1175/2009JCLI3188.1.

Webster, P. J., 1981: Mechanisms determining the atmospheric response to sea surface temperature anomalies. *J. Atmos. Sci.*, **38**, 554–571, doi:10.1175/1520-0469(1981)038<0554:MDTART>2.0.CO;2.

Wu, Q., and Q. Hu, 2015: Atmospheric circulation processes contributing to a multidecadal variation in reconstructed and modeled Indian monsoon precipitation. *J. Geophys. Res.*, **120**, 532–551, doi:10.1002/2014JD022499.